Hydraulic Resistance in Rock-Ramp Fish Passes for Various Shapes of Macroroughness

Ludovic Cassan, Flavia Cavalcanti Miranda, Pascale Laurens

Hydraulic resistance in rock ramp fish passes for various shapes of macro-roughness

LUDOVIC CASSAN[1], FLAVIA C. MIRANDA[2], and PASCALE LAURENS[3]

[1]*Institut de Mécanique des Fluides, Université de Toulouse, Toulouse INP, Allée du Professeur Camille Soula, Toulouse 31400, France*, *Email: lcassan@imft.fr*
[2]*Institut de Mécanique des Fluides, Université de Toulouse, Toulouse INP, Allée du Professeur Camille Soula, Toulouse 31400, France*, *Email: fcavalcantim@gmail.com*
[3]*Institut de Mécanique des Fluides, Université de Toulouse, Toulouse INP, Allée du Professeur Camille Soula, Toulouse 31400, France*, *Email: pascale.laurens@imft.fr*

ABSTRACT

The objective of this study is to improve the design criteria of rock ramp fish passes by better describing the physics of frictional phenomena such as the impact of the deformation of the free surface or the bed shear stress due to the presence of obstacles. Experiments on square-shaped obstacles were performed in a scale model. A new analysis of the old and current measurements allowed to specify the calibration coefficient of the drag and bottom friction forces. For a given water depth, the flow rate accuracy is about 10 % by using only three parameters per shape. Thus, a more precise comparison of the flows according to the shape of the obstacles could be carried out. This plays an important role for the specification of projects of equipment of river dams. The theoretical advantages of each shape were highlighted, such as, the significant reduction of the maximum velocity for the configuration with square obstacles.

INTRODUCTION

In order to restore ecological continuity in rivers, one possible option is to equip low-head weirs with rock ramps (Larinier et al. 2006; Katopodis et al. 2001). For the last ten years, this type of structure has been experimentally (Baki et al. 2014; Golpira et al. 2020; Cassan et al. 2014; Muraoka et al. 2017) and numerically (Chorda et al. 2019; Miranda et al. 2013; Baki et al. 2016; Amaral et al. 2019) studied for specifying the hydrodynamic conditions which could facilitate or prevent fish passage. In most cases, obstacles are concrete cylinders or natural rocks for simplifying their construction. According to Baki et al. (2014), several stage-discharge relationships have been proposed for this passage type with natural rocks. Cassan et al. (2014) proposed a methodology

for estimating the stage-discharge relationships of a rock ramp fish pass with emergent boulders by varying the obstacle density and shapes. Both methods are based on the estimation of the block drag coefficient to quantify hydraulic resistance as a function of the bulk velocity. In Cassan and Laurens (2016), the stage-discharge relationships were extended for arrangements with different spaces in longitudinal and transversal direction in emergent and submerged cases , i.e., obstacles piercing or not the free surface. However, the stage-discharge relationship and maximum velocity, named as design criteria, given in Cassan and Laurens (2016) are derived from those of Cassan et al. (2014) without being recalibrated to take into account for possible variation in obstacle density. Furthermore, no validation on square shaped obstacles has yet been performed. Therefore, it is necessary to verify the validity of these laws for all possible obstacle shapes and for shallow water depth relative to the block diameter since these ratios can be encountered in real fishways.

The purpose of this article is to explain the expressions of the block drag coefficients described in Cassan and Laurens (2016). They had been obtained by experimental correlations that were not physically based on knowledge of flows. Here, the pressure distribution around the blocks and the energy dissipation in the boundary layer at the bottom (including horse shoe vortex and roughness size influence) are taken into account and scaled with appropriate parameters. The second objective is to validate this physically based approach for different block shapes. For the description of the block drag coefficients, this paper relies on the fine flow descriptions available in (Tran et al. 2016; Golpira et al. 2020; Chorda et al. 2019; Miranda et al. 2013). The calibration is performed on the basis the experimental measurements given in (Cassan et al. 2014; Cassan and Laurens 2016; Miranda et al. 2013) as four shapes are then available with several diameters and block spacing. In addition, for the validation, a new set of experiments with square blocks was performed on a scale 1:2 rock ramp fish pass.

EXPERIMENTAL SETUP

A new series of measurements was carried out in a tilting channel equipped with blocks 0.34 m high and 0.18 m side length(Fig. 1). The channel is 12 m long and 1 m width. The blocks, which are square in shape, are staggered and spaced at a constant distance (center to center) of 50 cm in the longitudinal (a_x) and transverse (a_y) directions. Thus, it is possible to define a density $C = D^2/a_x a_y$, where D is a characteristic width facing the flow (e.g., block side length).

The bottom of the channel is covered with pebbles with a characteristic k_s size of 4 cm. Here k_s refers to the d_{50} of the granular distribution to be consistent with the formula used for the bottom friction (Rice et al. 1998). Experimentally, the water height is measured with a ruler from the rigid bottom of the channel. Next, the roughness height k_s is then subtracted from the measurements. The considered obstacle is located 5 m from the upstream entrance at the center of the channel transversaly. A measurement of the water height is made at the center of the upstream face $h_{\max}$ and another on the downstream face $h_{\min}$ (Fig. 1). These two values are the maximum and the minimum waterdepth on the area $a_x * a_y$ respectively. The mean height h is obtained by averaging these two values. The water depth was measured for 20 trials that were the combination of four discharges ($Q = 20, 40, 60$ and 80 l/s) and five slopes (1, 2, 3, 4, 5 %). The

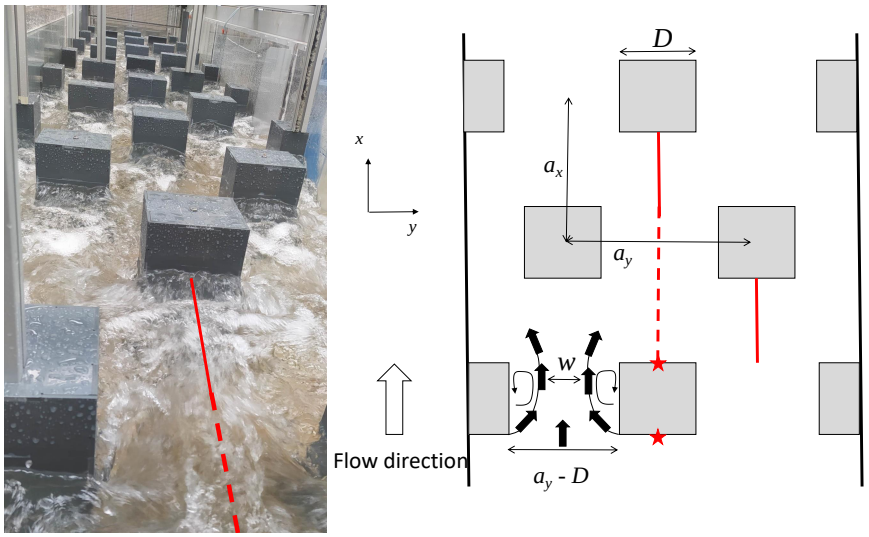

Fig. 1. Experimental device with square blocks (left) and schematic top view (right). The stars represent the position of the water depth measurements.

blocks are emergent for all experiments.

THEORETICAL BACKGROUND

Hydraulic friction in a fishway is calculated using the momentum balance around one obstacle. The drag coefficient reproducing the force of the block on the water is assumed to be close to that of a two-dimensional flow but with corrections due to particularities of the free surface, the steep slopes or/and the presence of the bed. The works of Cassan et al. (2014) and Cassan and Laurens (2016) specify these corrections. The case of flat-faced obstacles is treated specifically (only for trapezoidal shape) in Cassan et al. (2014). It can be noted that the proposed correction functions are only validated for circular blocks in the study of Cassan and Laurens (2016). The following analysis should generalize this approach for planar faces and, in particular, for square shapes.

Additional force due to bed interaction

The total frictional force is modeled by Eq. (1) where the first term in the right hand side corresponds to bed friction (Cassan et al. 2014) and the second term is the additional force due to interaction between flow and obstacle,

$$F_{bed} = \frac{1}{2}\rho C_f a_x a_y V^2 + \frac{1}{2}\rho C_b D^2 V^2, \tag{1}$$

where C_f is the friction coefficient obtained either by Blasius law (smooth regime) (Cassan et al. 2014) or by Rice law (Rice et al. 1998) (rough flow), V and ρ are the bulk velocity and the water density, respectively. To account for the effect of obstacles, a coefficient C_b is introduced. It can be attributed to Horse Shoe Vortex or other flow accelerations around an obstacle (Sadeque et al. 2008) that may be responsible for scour (Zhao et al. 2010). The stress can be three times greater locally than for an flow without

obstacle. Thanks to this coefficient, the additional friction force is modeled as a function of the average kinetic energy. The bed shear stress is assumed to be applied on an area equivalent to D^2, as suggested by the results of Golpira et al. (2020). Thus, as the density, $C = D^2/a_x a_y$, decreases, this contribution is relatively small compared to the total friction on the bottom.

The dimensionless expression for the frictional force can be rewritten as

$$\frac{F_{bed}}{\rho g h a_x a_y} = \frac{1}{2}\left(C_f + C_b C\right) F_0^2, \tag{2}$$

where g is gravitational acceleration, h corresponds to the water depth and F_0 is the Froude number based on the bulk velocity V ($F_0 = \frac{V}{\sqrt{gh}}$).

Additional force due to the free surface

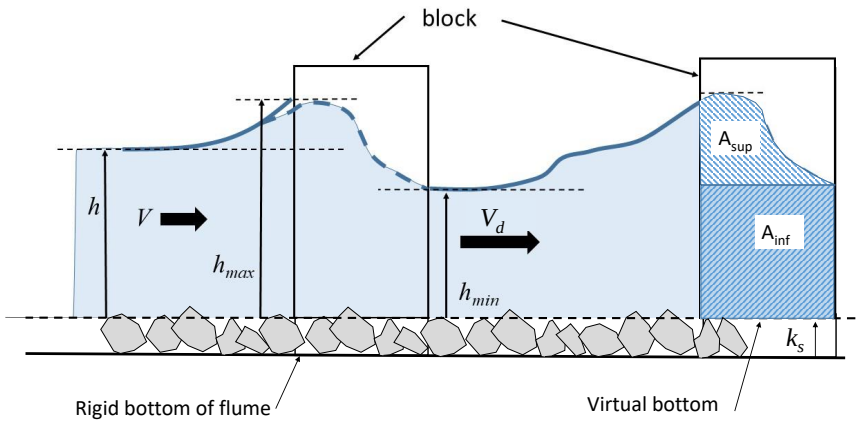

Fig. 2. Side view of the flow pattern and description of involved hydraulic parameters. The water profile is drawn along red lines on Fig. 1.

The description of the additional force on the obstacle is done here based on the work of Fenton (2008). In order to understand the effects of the different geometrical terms, the diagram shown in Fig. 2 is considered. The presence of an obstacle necessarily implies a variation in height (Δh) between upstream ($h_{\max}$) and downstream ($h_{\min}$) as a function of Froude number F. The representative Froude number of the flow is based on the average velocity between the blocks V_g ($F = V_g/\sqrt{gh}$), with $V_g = \frac{V}{1-\sqrt{\frac{a_x}{a_y}C}}$.

The free surface deformation denoted Δh is scaled by applying Bernoulli's theorem between the upstream face and the contracted section where $h = h_{\min}$ (Cassan et al. 2014), which gives

$$\frac{\Delta h}{h} = \frac{1}{2} F^2 r^2 \left(\frac{h}{h_{\min}}\right)^2, \tag{3}$$

where r is the ratio between the lateral width of the jet (w) and the distance between the blocks ($a_y - D$) (Fig. 1). Because of the continuity equation, r is also the ratio of the

maximum velocity denoted $V_{\max}$ and V_g. Neglecting the viscous drag, the drag force of the block along the x axis can be expressed as follows

$$F_{drag} = \int_{A_{inf}} -p\vec{n}ds\vec{e}_x + \int_{A_{sup}} -p\vec{n}ds\vec{e}_x, \tag{4}$$

where p is the static pressure, $\vec{n}$ is the surface normal vector, ds is surface element and $\vec{e}_x$ corresponds to the unit vector along the x axis. The contact surface between the block and the water A is composed of a lower part A_{inf} from the bottom to $h_{\min}$ and a near-surface part A_{sup} (Fig. 2).

The first term of the right hand side of Eq. (4) is modeled by a classical drag term based on the velocity V_g. The acceleration due to vertical contraction is accounted for using the continuity equation applied between the blocks and the downstream of the block, i.e $V_d = (h/h_{\min})V_g$. Previous works of Cassan and Laurens (2016) have shown that replacing V_g by the bulk velocity V compensates for the concentration-related wake hidden effects.

The last term of Eq. (4) is modeled assuming a hydrostatic pressure. In the case of a square block, with a constant height over the width, but different in the upstream and downstream direction, this term can be written as $\rho g D h \Delta h$ (Fenton 2008). For the case of an arbitrary shape, this term can be rewritten by introducing the coefficient C_s.

The value of C_s thus depends on the pressure distribution around the obstacle in the near-surface area A_{sup}. For a square block C_s is therefore 1 if a hydrostatic distribution is considered on the upstream and downstream face. In this paper, C_s is obtained by using experimental data to obtain an averaged value available for a wide range of hydrodynamic conditions ($0.2< F<1$, $0.08<C< 0.2$, $0.01< S<0.07$ and $0.3 < h/D<1$) which are possible in a real design process. By replacing the two terms in Eq. (4), the total drag force scaled by the weight is then given as

$$\frac{F_{drag}}{\rho g h a_x a_y} = \frac{1}{2} C_{d0} C h^* \left(\frac{h}{h_{\min}}\right)^2 F_0^2 + C_s C h^* \frac{\Delta h}{h}, \tag{5}$$

in which C_{d0} corresponds to the drag coefficient for a 2D single-phase case (infinitely high and without free surface), and $h^* = h/D$.

Flow description

Three types of flows can be distinguished:

- subcritical, when all the points of the flow are such that the local Froude number is lower than 1.
- critical, when the regime transition appears because of an accelerated jet which goes on the downstream obstacle by creating a hydraulic jump. For this critical regime, $h_{\min}/h = F^{1/3}$ is assumed (Cassan et al. 2014).
- supercritical, when the average height between blocks is lower than the critical height. This behavior is possible when the water depth is small compared to the space between blocks. The flow is mainly governed by the friction at the bottom.

In the subcritical case, Eq. (3) has already been verified in Cassan et al. (2014) and Tran et al. (2016), leading to (with $a_x = a_y$)

$$\frac{F_{drag}}{\rho g h a_x a_y} = \frac{1}{2} C_{d0} C h^* \left(\frac{h}{h_{\min}}\right)^2 \left(1 + \frac{2C_s r^2}{C_{d0}\left(1-\sqrt{C}\right)^2}\right) F_0^2. \tag{6}$$

The supercritical case is not sought in a fishway because the water depth is too shallow and velocity is too fast for the passage. Nevertheless, to evaluate the flow rate in this case, the additional surface stress can be neglected and the calculation of the stage-discharge relation remains valid but the bottom friction is then preponderant over the drag force.

For the critical case, the analysis done in Cassan et al. (2014), which allows to obtain a continuous transition of the stage discharge relationship between the subcritical and supercritical cases is then considered here. This transition is based on a physical assumption that there is a regime transition between the accelerated and contracted flow and the next row of blocks. Thus, a critical velocity and height exist here. Therefore, the drag force is based on these two hydrodynamic quantities.

Cassan et al. (2014) proposed a function $f(F)$ to model the continuous transition between the three behaviors. It gives a limiting Froude number of regime change as a function of the shape of the block. In order to keep consistency between the methods (the present and the one of Cassan et al. (2014)), we propose to merge the two drag terms into one,

$$\frac{F_{drag}}{\rho g h a_x a_y} = \frac{1}{2} C_{d0} C h^* f(F) F_0^2, \tag{7}$$

with the function $f(F)$ computed as $f(F) = \min\left(\frac{r_2}{1-\frac{1}{4}F^2}, \frac{1}{F^{2/3}}\right)^2$, where r_2 is a coefficient representing the additional surface force. It is expressed as

$$r_2 = \left(1 + \frac{2C_s r^2}{\left(1-\sqrt{C}\right)^2 C_{d0}}\right)^{0.5}. \tag{8}$$

To take into account the supercritical case, $f(F)$ is set equal 1 if $F > 1$. Thus, the additional surface force is neglected because the experimental correlation for Δh is no longer valid.

Momentum balance

The equation of momentum in steady state can be given as the drag and friction forces at the bottom equals to the water weight, because the variation of momentum is zero. It gives,

$$\frac{1}{2}\left(C_f + C_b C\right) F_0^2 + \frac{1}{2} C_{d0} C h^* f(F) F_0^2 = S, \tag{9}$$

where S is the bed slope.

The term $C_b C F_0^2$ in Eq. (9) which is due to the bottom shear stress is then associated with the drag force. This has the advantage of gathering all the terms related to the

Table 1. Parameters based on the shape of the obstacles according to the experimental results

shape	D (mm)	C	C_{d0}	C_b	C_s	C_s with $C_b = C_{d0}$	r
rounded face	125	0.13	1.3	1.36	0.044	0.11	1.2
trapezoidal face	125	0.13	2.2	2.5	0.25	0.3	1.6
cylinder	115	0.13	1	1.1	0.03	0.043	1.1
square	115	0.13	2	2.5	0.10	0.15	1.5

presence of the obstacles. This way, consistency is given with the studies of Cassan and Laurens (2016) but also with the models based only on a drag coefficient of Baki et al. (2014). Thus, Eq. (9) becomes

$$\left(C_f + C_{d0} C h^* f(F) f(h^*)\right) F_0^2 = 2S, \tag{10}$$

where

$$f(h^*) = 1 + \frac{C_b}{C_{d0} f(F) h^*}. \tag{11}$$

This expression is close to the one found in Cassan et al. (2014) and Cassan and Laurens (2016) but here the coefficients of $f(h^*)$ depend on the shape of the obstacle since the previous formulation was $f(h^*) = 1 + \frac{1}{(h^*)^2}$.

MODEL CALIBRATION

The use of Eq. (10) requires the calibration of the constants C_s and C_b. This will be done here using the experiments and simulations obtained in Cassan et al. (2014) and Miranda et al. (2013). These experiments were performed with 12 cm diameter circular and square wood blocks, respectively. The density C was 13%. The calibration of these constants is performed by minimizing the root mean square deviation of the normalized flow rates between calculated and measured flow. Table 1 shows the optimized values for each of the four shapes tested, for which only the most accurate data ($h > 5$ cm) were used. The trapezoidal face refers to a trapezoidal shape with the larger width fixed on the upstream side (Cassan et al. 2014). The rounded face corresponds to the trapezoidal one but with a half circular shape placed on the upstream face (Cassan et al. 2014).

As expected, the values of the constants C_b and C_s, presented in Table 1, evolve in a similar way as C_{d0}. Indeed, the more the shape of the front face becomes flat, the more the shear stress on the bottom increase. The detachment on the upstream edges causes more dissipation in the bed area. Similarly for rounded shapes, the pressure difference at the surface is smaller between the upstream and downstream faces. Moreover, considering the accuracy of the chosen measurements and the high sensitivity to C_b, a second step is performed to fix the value of C_b from the approximation C_b=C_{d0}.

Once C_s is obtained, it is possible to know the evolution of the parameter r_2 for each obstacle shape, density C and Froude number F (Eq. (8)). As it can be seen in Fig. 3, for round and square shapes, the average values of r_2 are 1.1 and 1.4 respectively. It can be

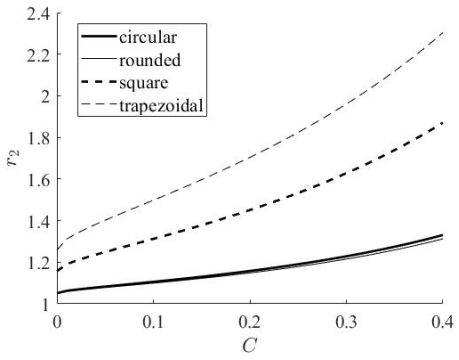

Fig. 3. Evolution of the parameter r_2 as a function of the density C and shape. For each obstacle shape, the parameters are set according to those found in the table 1.

observed in Fig. 4 that the parameterization obtained for the cylinders allows to estimate the flow rate with a deviation of lower than 10 %. This deviation corresponds to the expected uncertainty of the discharge calculation if a 5 mm water height measurement error is considered. Only the cases for supercritical flows have a larger deviation.

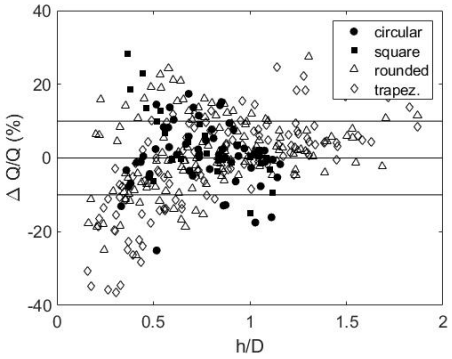

Fig. 4. Difference between measured and calculated flow discharges as a function of the relative height. The continuous lines represents an error of 10%.

A new set of experimental measurements, presented in section two, was used to validate both Eq. (9) and the proposed calibration for the square blocks. Regarding the discharge, Eq. (10) allows its estimation with an error of 10 %, which is similar to the error obtained in the calibration process (Fig. 5). Then, the validation of the design relationship is obtained for square blocks at a larger scale.

RESULTS: IMPLICATION FOR FISH PASSAGE

The maximum possible velocity in the fishway is a key parameter for its proper design because it determines wether a structure will be potentially passable by a given species. Concerning circular blocks, experiments of Cassan et al. (2014) and numerical simulations of Tran et al. (2016) have shown that the use of averaged velocity V_g allowed to have a good estimation of the real maximum velocity. It is now necessary to investigate

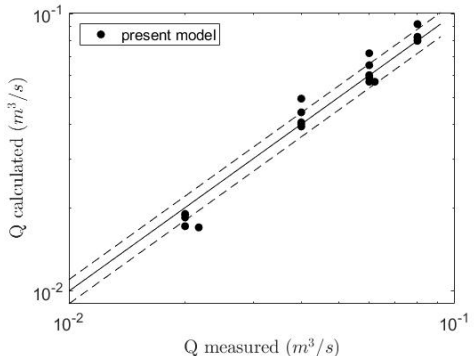

Fig. 5. Difference between measured and calculated discharges as a function of the relative height. The dotted lines represent a difference of 10 %.

the effect of the different shapes because they imply a different lateral contraction of the jet. For this reason, Cassan et al. (2014) introduced a coefficient r which is the ratio between the maximum and minimum velocities, $V_{\max}$ and V_d respectively. Indeed V_g and V_d are not equal because of the vertical contraction and their ratio is given by $\sqrt{f(F)}$ (Eq. (3)). Moreover, considering Table 1 and Fig. 3, the ratio r is close to r_2 for the four analysed shapes. Thus, a relation for $V_{\max}$ can be obtained from the parameters r, $f(F)$ and V_g by rewriting Eq. (3) in terms of $f(F)$ instead of $\Delta h/h$,

$$r = \frac{V_{\max}}{V_g} = \sqrt{f(F)}. \tag{12}$$

A first value of r is retained and is given in Table 1, for practical use it can be approximated by the law $r = 0.4C_{d0} + 0.7$. With square blocks, the discharge is significantly reduced for the same water depth, as depicted in Fig. 6. The ratio of discharges is close to the square root of the ratio of C_d, which is also the ratio of velocities V_g in both cases if the lateral contraction would have been neglected. It is observed that for the water depth of 30 cm, the velocity of 1.5 m/s is obtained with a slope of 3 % for the circular blocks while it occurs for a slope of 5.5 % for square blocks. In general, Fig. 6 shows that the same velocity can be reached with a steeper slope for square obstacles and, therefore, the fish pass could be shorter, leading to a reduction of building costs. Thus, the interest of the square blocks is significant even if the attractiveness of the fish pass is reduced. Solutions such as side slopes could compensate the loss of attractiveness of square blocks by locally increasing the flow velocity.

It can be assumed that for steep slopes, the high energy dissipation upstream of the blocks could prevent the fish passage. The power dissipation for the proposed configurations is plotted in Fig. 7. This graph shows significant dissipated power for fish passage once the slope exceeds 5 %. For instance, the limit for holobiotic species is estimated at 300 W/m^3 (Larinier et al. 2006). However, for the same water depth, the dissipated power per volume for square blocks is lower than for cylinders because of the lower flow rates and the higher water depths.

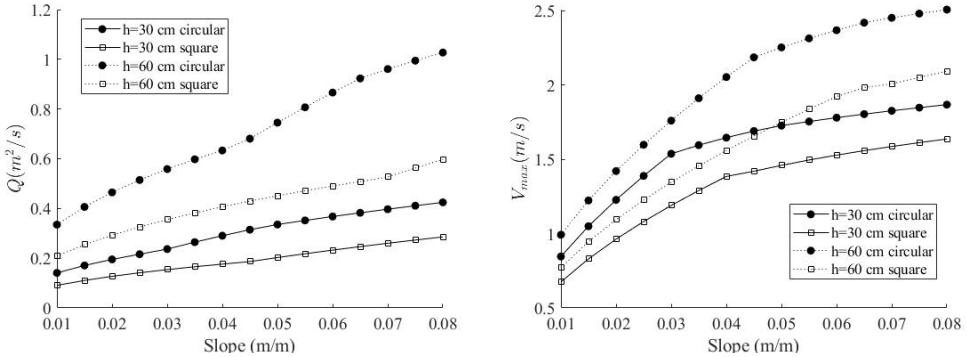

Fig. 6. Comparison of discharge per unit width (left) and maximum velocity (right) for a pass with C = 13 % and D = 50 cm.

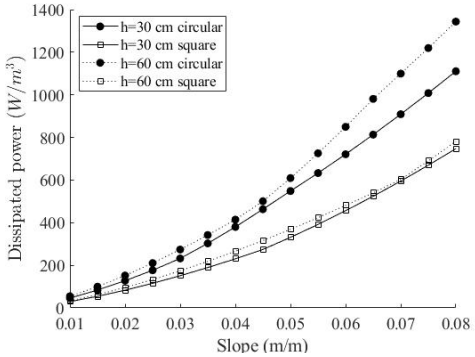

Fig. 7. Average power dissipation for a fish pass with C = 13 % and D = 50 cm.

CONCLUSION

The design laws of rock-ramp fish passes have been improved with a more physical model to better take into account the impact of the shape of the obstacles. The parameters of the drag coefficient correction laws were based on a physical interpretation, even if a calibration was necessary to refine the predictions. The proposed laws for circular obstacles were not significantly modified, while the laws for the square obstacles have been adjusted. The calibration of parameters were done with results from the literature, whereas their validation was performed with new experimental data. The good agreement between experimental and theoretical results leaded to a more realistic comparison between the two shapes. For the same slope and density, the configuration with square blocks decreased drastically the flow velocity compared to one with circular obstacles. This shape is the one likely to provide a better fish passage efficiency. The theoretical advantage of the square obstacles on fish passage should be evaluated in the future experiments including the fish behavior.

Data Availability Statement

All data, models, or code that support the findings of this study are available from the corresponding author upon reasonable request.

REFERENCES

Amaral, S. D., Quaresma, A. L., Branco, P., Romão, F., Katopodis, C., Ferreira, M. T., and Santos, A. N. (2019). "Assessment of retrofitted ramped weirs to improve passage of potamodromous fish." *Water*, 11, 1–10.

Baki, A., Zhang, W., Zhu, D., and Rajaratnam, N. (2014). "Mean flow characteristics in a rock-ramp-type fish pass." *Journal of Hydraulic Engineering*, 140(2), 156–168.

Baki, A., Zhang, W., Zhu, D., and Rajaratnam, N. (2016). "Flow simulation in a rock-ramp fish pass." *Journal of Hydraulic Engineering*, 142(10), 04016031.

Cassan, L. and Laurens, P. (2016). "Design of emergent and submerged rock-ramp fish passes." *Knowl. Manag. Aquat. Ecosyst.*, 417, 1–10.

Cassan, L., Tien, T., Courret, D., Laurens, P., and Dartus, D. (2014). "Hydraulic resistance of emergent macroroughness at large froude numbers: Design of nature-like fishpasses." *Journal of Hydraulic Engineering*, 140(9).

Chorda, J., Cassan, L., and Laurens, P. (2019). "Modeling steep-slope flow across staggered emergent cylinders: Application to fish passes." *Journal of Hydraulic Engineering*, 145(11), 1–14.

Fenton, J. (2008). "Keynote lecture, pp 15-22 of hydraulic structures." *Proc. 2nd International Junior Researcher and Engineer Workshop on Hydraulic Structures.*, S. Pagliara, ed., AIHR, University of Pisa., Edizioni Plus, 15–22.

Golpira, A., Baki, A., and Zhu, D. (2020). "Higher-order velocity moments, turbulence scales and energy dissipation rate around a boulder in a rock-ramp fish passage." *Sustainability*, 12, 5385.

Katopodis, C., Kells, J., and Acharya, M. (2001). "Nature-like and conventional fishways: Alternative concepts?." *Canadian Water Resources Journal / Revue canadienne des ressources hydriques*, 26(2), 211–232.

Larinier, M., Courret, D., and Gomes, P. (2006). "Technical guide to the concept on nature-like fishways." *Rapport GHAAPPE RA.06.05-V1*, 5 In French.

Miranda, F., Cassan, L., Laurens, P., and Tran, T. (2013). "Study of a rock-ramp fish pass with staggered emergent square obstacles." *Water*, 13, 1175.

Muraoka, K., Satoru Nakanishi, S., and Kayaba, Y. (2017). "Boulder arrangement on a rocky ramp fishway based on the swimming behavior of fish." *Limnologica*, 62, 88–193.

Rice, C. E., Kadavy, K., and Robinson, K. (1998). "Roughness of loose rock riprap on steep slopes." *Journal of Hydraulic Engineering*, 124(2), 179–185.

Sadeque, F., Rajaratnam, N., and Loewen, M. (2008). "Flow around cylinders in open channels." *Journal of Engineering Mechanics*, 134(1), 60–71.

Tran, T., Chorda, J., Laurens, P., and Cassan, L. (2016). "Modelling nature-like fishway flow around unsubmerged obstacles using a 2d shallow water model." *Environmental Fluid Mechanics*, 16(2), 413–428.

Zhao, M., Cheng, L., and Zang, Z. (2010). "Experimental and numerical investigation of local scour around a submerged vertical circular cylinder in steady currents." *Coastal Engineering*, 57, 709–721.